Supporting Information

Multi-effective Nanoplatform with Down/Upconversion Dual-mode Emissions for NIR-II Imaging and PDT/PTT Synergistic Therapy of Early Atherosclerosis

Wen Gao,[a] Lijun Lv,[a] Guanghan Li,[a] Hongxiu Zhao,[a] Jia Zhou,[c]* Yuan Cheng,[a]* and Bo Tang[a,b]*

[a]College of Chemistry, Chemical Engineering and Materials Science, Key Laboratory of Molecular and Nano Probes, Ministry of Education, Collaborative Innovation Center of Functionalized Probes for Chemical Imaging in Universities of Shandong, Institutes of Biomedical Sciences, Shandong Normal University, Jinan 250014, China.

[b]Laoshan Laboratory, Qingdao 266237, Shandong, China.

[c]Shandong Provincial Hospital Affiliated to Shandong First Medical University: Shandong Provincial Hospital.

Corresponding Authors.

E-mail: tangb@sdnu.edu.cn, chengyuan@sdnu.edu.cn, zhoujia@sdfmu.edu.cn.

Table of Contents

1. Experimental Section..... S3
2. Material analysis..... S12
3. Supporting Figures..... S14

1. Experimental Section

Materials

Cerium chloride ($CeCl_3·6H_2O$), ytterbium chloride ($YbCl_3·6H_2O$), neodymium chloride ($NdCl_3·6H_2O$), erbium chloride ($ErCl_3·6H_2O$), ammonium fluoride (NH_4F), tetraethyl orthosilicate (TEOS), 3-aminopropyltriethoxysilane (APTES), fluorescein isothiocyanate (FITC), citric acid ($C_6H_8O_7·H_2O$) were obtained from Sigma-Aldrich (St. Louis, MO, USA). Ammonia (NH_4OH), ethanol (C_2H_6O) were purchased from Sinopharm Chemical Reagent. Co. Ltd. (Shanghai, China). 4% paraformaldehyde, Triton X-100 were purchased from Solarbio (Beijing, China). PBS, DMEM, and fetal bovine serum (FBS) were purchased from VivaCell Biosciences Ltd (Beijing, China). Cell Counting Kit-8 (CCK-8) and DAPI were obtained from Beyotime Biotechnology (Shanghai, China). Anti-CD36 and TRITC Conjugated AffiniPure Goat Anti-rabbit IgG were obtained from Boster (Wuhan, China).

Synthesis of CeO_2:Nd precursor.

CeO_2:Nd precursor was synthesized by the sol-gel method. $CeCl_3·6H_2O$ was dissolved in water to form a cerium salt solution. Then $NdCl_3·6H_2O$ and citric acid were added to the above solution, while PH was adjusted to 6 with ammonia. The mixed system was heated to 80 ℃ (5 ℃/min). After reaction, the gel was natural cooled and ground obtaining the CeO_2:Nd precursor.

Synthesis of CeO_2:Nd@SiO_2.

CeO_2:Nd@SiO_2 was synthesized by a modified versatile Stöber sol-gel method. Precursor powders (0.3 g) were dispersed in ethanol (40 mL) and distilled water (10 mL), and sonicated for 30 min with CO-520. Subsequently, ammonia (320 μL, 30%) and TEOS (0.5 mL) was added to the system. The mixture was stirred continuously for 24 h at room temperature. Finally, it was centrifuged and washed three times with ethanol. The above powders were further calcinated in air with a ramp of 5 °C/min to 600 °C for 2 h.

Synthesis of DC/UCNPs@SiO_2-RB/MB.

RB and MB were coated on the surface of DC/UCNPs with aminated silica shell, as follows in detail. CeO_2:Nd@SiO_2@CeO_2:Yb,Er (150 ppm) in distilled water (10 mL) was added into a 20 mL glass bottle. After sonicated for 10 min, CO-520 (1.2 mL) was slowly

added and sonicated for another 30 min. Then, ammonia (320 μL, 30%) was added and stirred for 1 h. Subsequently, TEOS (0.5 mL) was added and stirred for 2.5 h. Then, APTES (18 μL), RB (1 mg) and MB (1 mg) was added and incubated for 15 h under vigorous stirring. Finally, it was centrifuged and washed three times with ethanol.

Synthesis of DC/UCNPs@SiO_2-RB/MB/CD36.

DC/ UCNPs@SiO_2-RB/MB/CD36 was synthesized through a simple condensation reaction between the carboxyl group of the antibody and the amino group on the surface of the NPs. EDC (8.4 μmol) and NHS (8.4 μmol) were added to the solution of CeO_2:Nd@SiO_2@CeO_2:Yb,Er@SiO_2-RB/MB (1 mg·ml^{-1}, 10 mL) for catalysis, and then CD36 antibody (4 μg) was added with mild stirring for 12 h. The amino group on the surface of nanoparticles and the carboxyl group on the antibody formed amide bond through condensation reaction.

DC/UC Luminescence performance of DC/UCNPs@ SiO_2-RB/MB/CD36.

DC/UC emissions were all measured on a FLS-1000 Edinburgh fluorescence spectrometer using near infrared plus lasers (808 nm, 980 nm) with a 1.0 cm quartz pool and a slit width of 5.0/5.0 nm.

Characterization of as-prepared nanoparticles.

The morphology was characterized by an electron transmission electron microscope (HT7700 electron microscope, Japan) and a high-resolution transmission electron microscope (JEM-2100, JEOL, Japan). X-ray powder diffraction diagram (XRD) was measured via an X-ray powder diffractor (smart labse, Rigaku Denki Co., Ltd.). X-ray photoelectron energy spectroscopy (XPS) was measured by ESCALAB 250xi (Thermo Fisher, USA). Fourier Transform infrared (FT-IR) spectra was collected in a Nicolet Impact 410 FTIR spectrometer, Range is 400-4000 cm^{-1}. Zeta potential was detected on a Nano-ZS90 nanogranularity potentiometer. The protein spectra were characterized by SDS-PAGE gel electrophoresis.

Stability of DC/UCNPs@SiO_2-RB/MB/CD36.

DC/ UCNPs@SiO_2-RB/MB/CD36 was dissolved in PBS buffer (pH = 7.4), fetal bovine serum (FBS), and cell culture medium (adding 10% FBS to DMEM) and maintained for two weeks. Changes in the Zata potential at day 0, 2, 4, 6, 8, 10, 12 and 14 were examined.

Photothermal performance of DC/UCNPs@SiO_2-RB/MB/CD36.

Concentration gradient of DC/UCNPs@ SiO_2-RB/MB/CD36 (0-1 mg·mL^{-1}) was dispersed in PBS buffer, irradiated at 808 nm NIR (0-4.99 W·cm^{-2}) with different laser powers. Thermal images of the solution were captured by FLIR S6 infrared thermal imager (FLIR Systems Inc, USA), while the temperature changes were also recorded. In order to evaluate the reversibility of DC/UCNPs@ SiO_2-RB/MB/CD36 with light stimulation, 0.8 mg·mL^{-1} DC/UCNPs@SiO_2-RB/MB/CD36 in 10 light cycle experiments were carried out under the irradiation of 808 nm NIR at 4.99 W·cm^{-2} (laser irradiation for 30 seconds and natural cooling for 90 seconds were regarded as one cycle), and the temperature changes were measured and recorded.

Photodynamic performance of DC/UCNPs@SiO_2-RB/MB/CD36.

RDPP was chosen as the probe for the detection of O_2, and the fluorescence intensity of RDPP decreased with the increase of O_2 concentration. Aqueous solutions containing RDPP, H_2O_2 + RDPP, DC/UCNPs@SiO_2-RB/MB/CD36 + RDPP, DC/UCNPs@SiO_2-RB/MB/CD36 + H_2O_2 + RDPP were dripped into the respective tubes, and the concentrations of RDPP, DC/UCNPs@SiO_2-RB/MB/ CD36, and H_2O_2 were 5 mM, 0.1 mg/mL, and 10 mM, respectively. The fluorescence intensity of RDPP (λ ex = 560 nm) at 645 nm was recorded at predetermined time points.

DPBF was used as a probe to determine the ability of $^1O_2$ generation by detecting the quenching of DPBF fluorescence. Briefly, 2 μL of DPBF (3 mg·mL^{-1} in acetonitrile) was added into the solution of DC/UCNPs@SiO_2-RB/MB in distilled water (0.2 mL, 0.8 mg·mL^{-1}) and only DPBF in acetonitrile was used as the control. Two solutions were all continuously irradiated with a 980 nm laser at a power density of 1.2 W·cm^{-2} for 10 min, and the fluorescence of DPBF at 410 nm was recorded on a multi-modal microplate reader (RT6000) every 120 s. Meanwhile, experimental and control group solution kept in the dark were also measured and used as the corresponding dark control.

Cell culture.

Mouse macrophage RAW 264.7 cells and Normal human hepatocytes HL-7702 cells were obtained from the Committee on Type Culture Collection of Chinese Academy of Sciences. RAW 264.7 cells and HL-7702 cells were cultured in cell culture medium (DMEM containing 1% penicillin/streptomycin double antibody and 10% fetal bovine serum and medium). And placed in a 37 ℃, 5% CO_2 air-moist incubator (MCO-15AC, SANYO).

Cell viability assay.

The cell viability was detected by CCK-8 assay according to the manufacturer's protocol. After HL-7702 cells were digested with pancreatic enzyme and seeded overnight in cell suspension in 96-well plates. Incubating HL-7702 cells were supplemented with sterilized DC/UCNPs@SiO_2-RB/MB at different concentrations (0, 0.5, 0.4 and 0.8 mg·mL^{-1}) for 24 h. Then, 10 μL CCK-8 (take note not to produce air bubbles) was added to each well, and the incubation was continued for 1 h. Finally, the absorbance at 450 nm was measured by enzyme-linked immunosorbent assay (RT6000) and the cell survival rate was calculated.

In vitro targeting ability of DC/UCNPs@SiO_2-RB/MB /CD36.

We used flow cytometry to explore the targeting ability of DC/UCNPs@SiO_2-RB/MB/CD36 on RAW 264.7 cells. First, we prepared the fluorescein-labeled DC/UCNPs @SiO_2-RB/MB/CD36 and DC/UCNPs@SiO_2-RB/MB. Recover 0.5 mg DC/UCNPs@SiO_2-RB/MB/CD36 or DC/UCNPs @SiO_2-RB/MB in 5 mL PBS and then dissolve 0.2 mg FITC (λ ex/λ em = 494/518 nm) in 10 μL DMSO. Afterwards, the solution was added to the nanoparticles and gently stirred for 1 h at room temperature. Final centrifugation (1000 rpm, 10 min, 4 ℃) was washed several times with PBS/DMSO to remove the unreacted FITC.

The FITC-labeled DC/UCNPs@SiO_2-RB/MB/CD36 and DC/UCNPs@SiO_2-RB/MB (0.1 mg·mL^{-1}) were then jointly incubated with RAW 264.7 cells for 1 h, respectively. Cells were then washed three times with PBS to remove the remaining nanoparticles in the medium, cell digested and centrifuged (1000 rpm, 4 min) and redispersed in PBS buffer. Then fluorescence images were collected on Image Stream X cytometer (λ ex = 488 nm).

Unstained cells were compensated for fluorescence, and cell images were analyzed using the IDEAS ® image analysis software.

In vivo targeting ability of DC/UCNPs@SiO_2-RB/MB/ CD36. In order to study the biological distribution of as-prepared nanoparticles, FITC-labeled DC/UCNPs@SiO_2-RB/MB/CD36 and DC/UCNPs@SiO_2-RB/MB (10 mg·kg^{-1}) were injected into the tail artery of the $ApoE^{-/-}$ mice (n = 3). 2 h after injection, the distribution of nanoparticles was detected by histological analysis. 5 μm frozen section of the aortic root of $ApoE^{-/-}$ mice were sea by goat serum. The frozen sections were incubated with anti-CD68(1: 400) at 4 ℃ overnight, and then incubated with TRITC labeled secondary antibody at 37 ℃ for 1 h in the dark. After washing the secondary antibody with PBS buffer, DAPI counterstained the nucleus for 5 min. Finally, they were observed by TCS SP8 confocal laser scanning microscopy (Leica Co., Ltd. Germany).

Intracellular inhibition of ROIs.

RAW 264.7 cells were grown for one day and incubated with 10 μg·mL-1 DC/UCNPs@SiO_2-RB/MB/CD36 for 12 h. After incubation, cells were washed with phosphate buffer saline three times and incubated with 10 mM 2,7-dichlorofluorescein diacetate (DCFH-DA) at 37 ℃ for 30 min. Cells were then washed again and incubated with 1 mM H_2O_2 at 37 ℃ for 30 min. RAW 264.7 cells were harvested and the intensity of fluorescence was determined by flow cytometry. The ROI level was calculated as a ratio-mean intensity of experimental cells/mean intensity of control cells.

Intracellular production of O_2 and $^1O_2$.

Intracellular O_2 within RAW 264.7 cells were identified by RDPP. The hypoxic atmosphere was established by inoculating RAW 264.7 cells in culture medium containing $CoCl_2$ (200 μM) for 24h. Raw 264.7 cells were cultured as described above, stained with RDPP (100 μM) for 0.5 h and then stained with DC/UCNPs@SiO_2-RB/MB/CD36 (0.1 mg·mL^{-1}) for 60 min, then washed with PBS three times, and finally imaged with CLSM. RDPP was excited at 560 nm. The same concentrations of DC/UCNPs@SiO_2-RB/MB were used as a control.

Intracellular ROS was determined via DCFH-DA.

RAW 264.7 cells were operated by using the same procedure as cellular uptake and then sequentially incubated with DC/UCNPs@SiO_2-RB/MB and DC/UCNPs@SiO_2-RB/MB/CD36 for another 1 h. Raw 264.7 cells were continuously irradiated with a 980 nm laser at a power density of 1.2 W·cm^{-2} for 10 min. After that, DCFH-DA was added to the cells for 30 min. Next, RAW 264.7 cells were washed with PBS three times, and finally RAW 264.7 cells were observed with CLSM.

In vitro PTT/PDT therapeutic efficacy study.

In vitro cytotoxicity of DC/UCNPs@SiO_2-RB/MB/CD36 was determined by the CCK-8 assay according to the operating instructions. Raw 264.7 cells were cultivated in 96-well plates at a density of 2 × 10^5 cells per well for 24 h at 37 ℃. The DMEM solutions with DC/UCNPs@SiO_2-RB/MB/CD36 (0.8 mg·mL^{-1}) were dosed into each well for 1 h, and the cells were exposed to 808 nm laser irradiation at 4.99 W·cm^{-2} (laser irradiation for 30 s and natural cooled for 90 s were regarded as one cycle) for 10 light cycle or 908 nm laser at 1.2 W·cm^{-2} for 10 min. After that, 1μL of CCK-8 solution was added to each well for 1 h. Then RAW 264.7 cells were washed with PBS three times. Finally, an enzyme marker was used to test the absorption values. The cell viability (%) was calculated as the following Eq.:

$$\text{Cell viability (\%)} = [(A_1 - A_3)/ (A_2 - A_3)] \times 100\%$$

where A_1 is the absorbance of the experimental group, A_2 is the absorbance of the control group, and A_3 is the absorbance of the blank group.

Next, a Calcein-AM/PI assay was applied to evaluate the living and dead cells. Raw 264.7 cells were cultivated in confocal dishes for 24 h at 37 ℃. The experimental group was the same as the CCK-8 assay above. Cells were stained with Calcein-AM/PI for 30 min after being exposed to laser. Then RAW 264.7 cells were washed with PBS three times. Live and dead cells were distinguished by CLSM. Live cells were stained green, while dead cells exhibited red fluorescence. The stained cells were monitored by a fluorescent microscope.

Establishment of animal model.

ApoE$^{-/-}$ mice (6-8 weeks, male) were purchased from HFK Biotechnology Co. Ltd. (Beijing, China). Mice were fed ad libitum and housed under controlled lighting conditions (12 h light; 12 h dark). They were maintained under specific pathogen-free conditions. All animal care and experimental protocols complied with the Animal Management Rules of the Ministry of Health of the People's Republic of China and were approved by the Animal Care Committee of Shandong Normal University authorized by Shandong Experimental Animal Center. ApoE$^{-/-}$ mice were fed with a high-cholesterol diet to establish the atherosclerotic model.

In vitro and in vivo NIR-II imaging assessment.

DC/ UCNPs@SiO_2-RB/MB/CD36 were dispersed in 150 μL PBS buffer, and injected into ApoE$^{-/-}$ mice and Kunming mice (n = 3) through tail vein (10 mg·kg^{-1}) respectively. The NIR-II luminescence images were captured with IVIS Lumina III imaging system (FREDOR, China). A 0-20 W adjustable CW 808 nm laser (FREDOR, China) was used as an excitation source. The excitation light density was 1.2 W·cm^{-2}. The luminescent images were superimposed on bright-field images with ImageJ.

In vivo PTT/PDT therapeutic efficacy study.

ApoE$^{-/-}$ mice (6-8 weeks, male) were randomly divided into 6 groups (n = 18) and fed with high-fat feed (20% fat, 20% sucrose and 1.25% cholesterol). At the same time, mice were treated with six different treatments: (a) PBS; (b) PBS + NIR; (c) DC/UCNPs@SiO_2-RB/MB; (d) DC/UCNPs@SiO_2-RB/MB + NIR; (e) DC/UCNPs@SiO_2-RB/MB/CD36; (f) DC/UCNPs@SiO_2-RB/MB/ CD36 + NIR. DC/UCNPs@SiO_2-RB/MB and DC/UCNPs@SiO_2-RB/MB/CD36 were dispersed in 150 μL PBS buffer, and injected into mice through tail vein (10 mg·kg^{-1}) respectively. Mice in groups (a) and (b) were injected with the same volume of PBS buffer. Two hours later, the heart region of mice in groups (b), (d) and (f) was irradiated with 808 nm NIR (4.99 W·cm^{-2}) for 10 cycles and 980 nm NIR (1.2 W·cm^{-2}) for 10 min, and the spot diameter was 0.5 cm. Other groups were not exposed to NIR. These treatments were performed twice a week, and the weight of the mice was measured and recorded. After 12 weeks, all mice were collected serum, killed, dissected, and analyzed.

The evaluation of AS lesions degree in mice.

The aortic valve was analyzed histologically, and the aortic root was taken to the upper part of the heart, and the excess fat and connective tissue were removed, and then embedded and fixed. The slice thickness was controlled to be 5 μm, and continuous slices were made. When aortic valve structure appeared, the slices were formally reserved. The slices were stained with oil red O and hematoxylin, and the images were collected by NIS-Elements imaging software (Nikon, Japan). Finally, the plaque area percentage was calculated. And next, the artery was stained with oil red O, and the whole aorta of mice was taken out and the excess fat and connective tissue were removed. After longitudinal section, it was stained with Oil Red O. Using NIS-Elements imaging software to collect photos. And quantify the lesion area percentage in the vascular cavity.

ICP-AES analysis.

Plaque-bearing ApoE$^{-/-}$ mice were intravenously injected with 150 μL DC/UCNPs@SiO_2-RB/MB/CD36 PBS solution (10 mg·kg^{-1}). At 4 h postinjection, aortic arch, major organs and excretion were harvested immediately and weighed. Then these tissues and excretion were placed into borosilicate tube and digested in 70% w/v nitric acid containing 10 ppm Yttrium at 80 ℃ for 4 h. After cooled to room temperature, condensates were collected by centrifugation, and diluted to 5 mL with water. Samples were then filtered through a 0.45 μm hydrophilic PVDF membrane into 15 mL Falcon tubes. Standards were prepared by diluting 1000 ppm. cooper standards solution to 100 ppm, 10 ppm, 1 ppm, 0.2 ppm and 0.04 ppm with 15% w/v nitric acid. ICP-AES was performed on the samples using the Optima 7300 (Perkin Elmer).

Inflammatory cytokines assay.

The serum was collected from ApoE$^{-/-}$ mice with different treatments. ELISA kit was used to evaluate the levels of inflammatory-relative cytokines of tumor necrosis factor-α (TNF-α) and interleukin-1β (IL-1β) in the serum.

Biological safety.

In vivo toxicity analysis. The major organs (heart, liver, spleen, lung, kidney) of mice were collected, and H&E staining (hematoxylin and eosin) were used to evaluate the damage to mice major organs. Images were observed and collected by the DMI3000.

Statistical analysis.

Each experiment was repeated three times in duplicate unless stated otherwise. Data were presented as mean ± S.D. Comparisons between groups were analyzed using Student's t-test, $P < 0.05$ was considered statistically significant.

2. Material analysis

Characterization. CeO_2:Nd@SiO_2 (about 120 nm), DC/UCNPs (about 130 nm) and DC/UCNPs@SiO_2-RB/MB (about 200 nm) nanoparticles were all spherical and well dispersed (Figure S1). Besides, lattice stripes with a spacing of 0.312 nm were clearly observed in DC/UCNPs@SiO_2-RB/MB particles, which were consistent with the d111 spacing (0.311 nm) of CeO_2 hexagonal phase. However, the shell did not have lattice stripes, indicating that SiO_2 was successfully coated on the surface of nanoparticles (Figure S1f).

Plus, XPS patterns (Figure S2a) showed obvious characteristic peaks at 884.1 eV and 904.1 eV ($Ce3d_{5/2}$ and $Ce3d_{3/2}$, respectively) in CeO_2:Nd@SiO_2, DC/UCNPs and DC/UCNPs @SiO_2-RB/MB, while no characteristic peaks were observed in the precursor. In addition, besides the broadband from SiO_2, the main diffraction peak of CeO_2:Nd@SiO_2, DC/UCNPs and DC/UCNPs@SiO_2-RB/MB were all related to the crystalline phase of CeO_2 matrix [JCPDS card No. 34-0394] (Figure S2b). All the work proved the successful synthesis of DC/UC nanoparticles.

Moreover, the FT-IR spectrum (Figure S3a) and protein gel electrophoresis (Figure S3c) were also measured to confirm the modification of CD36 antibody. In addition to absorption peaks of Si-O-O bonds (approximately 1057 cm^{-1} in black line, 1035 cm^{-1} in red line, and 1054 cm^{-1} in blue line), there were two characteristic absorption peaks of NH-CO bonds (approximately 1644 cm^{-1} and 3265 cm^{-1}) indicating the successful modification of CD36 antibody. What's more, the protein band of DC/UCNPs@SiO_2-RB/MB/CD36 was located on the top of the protein gel owing to the weight of DC/UCNPs, while there was no protein band appeared in DC/UCNPs@SiO_2-RB/MB (Figure S3c). Coupled with the change of Zeta potential (Figure S3b), these results fully vindicated the successful synthesis of DC/UCNPs@SiO_2-RB/MB/CD36.

Further, DC/UCNPs@SiO_2-RB/MB/CD36 were dissolved in PBS buffer (pH 7.4), cell culture medium (DMEM), and serum (FBS) for two weeks, respectively. There were no significant changes in solution color and zeta potential, which demonstrated the excellent stability of as-prepared DC/ UCNPs@SiO_2-RB/MB/CD36 (Figure S4).

DC/UC Luminescence performance. In our work, under the excitation of 980 nm laser, DC/UCNPs produced strong green (525/550 nm) and red (650 nm) upconversion emissions (Figure S5a), while it also produced strong NIR II (1068 nm) downconversion emissions with 808 nm excitation (Figure S5b). Note here that the UC fluorescence intensity substantially increased when the ratio of Yb/Er increased from 15/1 to 25/1. Nevertheless, the UC fluorescence intensity gradually decreased when the ratio of Yb/Er exceeded 25/1. At the same time, the DC fluorescence intensity substantially increased when Nd^{3+} content increased from 5 to 25%, but subsequently decreased when the Nd^{3+} content exceeded 25%. Accordingly, it could be concluded that 25/1 was the optimum ratio of Yb/Er and 25% was the optimum concentration of Nd^{3+} to improve the UC and DC emission of as-prepared phosphors respectively.

The energy transfer mechanism of as-prepared phosphors was proposed in Figure S5c, which itemize here below. First to discuss is the UCL mechanism of Er^{3+} ions. Under the irradiation of 980 nm laser, electronic transitions of Yb^{3+} sensitizers from the ground state ($^2F_{7/2}$) to $^2F_{5/2}$ state were generated by absorbing the low-energy NIR photons. Due to the energy transfer from Yb^{3+} to Er^{3+}, Er^{3+} activators in the ground state ($^4I_{15/2}$) were activated into the excited state ($^4I_{11/2}$, $^4F_{7/2}$). Since Er^{3+} ions on $^4F_{7/2}$ state were instable and the distance between $^4F_{7/2}$ state and adjacent states was short enough, some Er^{3+} ions on $^4F_{7/2}$ state relaxed nonradiatively to $^2H_{11/2}$, $^4S_{3/2}$ state. Subsequently, Er^{3+} ions on $^2H_{11/2}$ state transferred to the ground state generating 525 nm emission. Concurrently, some Er^{3+} ions on $^4S_{3/2}$ state directly transferred to the ground state radiating 550 nm emission, while others relaxed nonradiatively to $^4F_{9/2}$ state and then transferred to the ground state yielding 650 nm emission. The next concern was the DCL mechanism of Nd^{3+} ions. Under 808 nm irradiation, electronic transitions of Nd^{3+} from the ground state ($^4I_{9/2}$) to $^4F_{5/2}$ state were generated, and then realized a rapid non radiation process to $^4F_{3/2}$ state. Subsequently, Nd^{3+} ions on $^4F_{3/2}$ state can decay to $^4I_{11/2}$ state through radiative transitions, followed with 1068 nm NIR II emission.

3. Supporting Figures

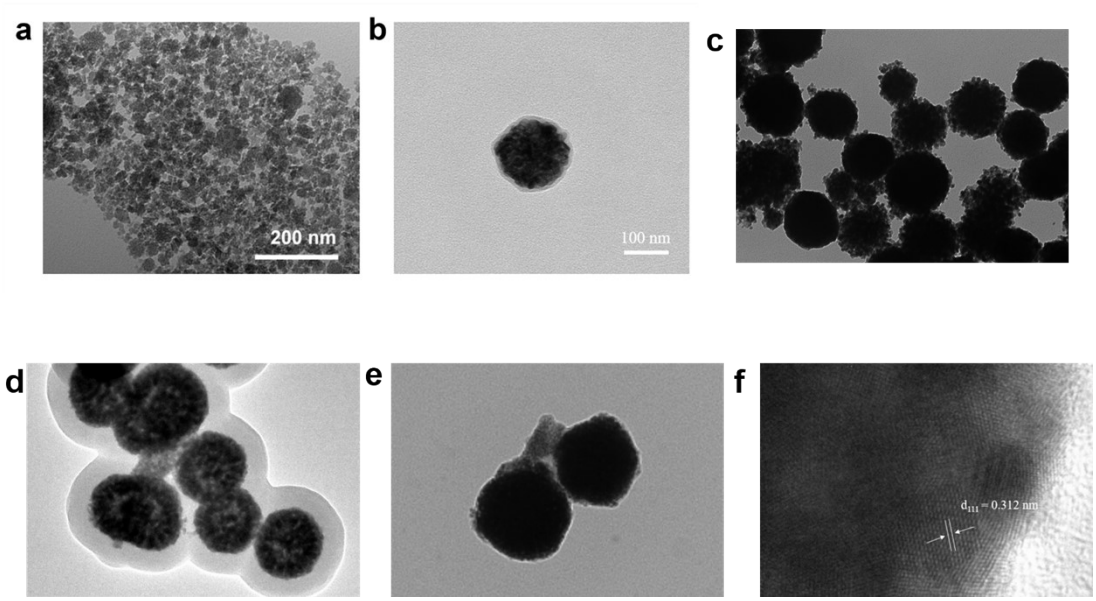

Figure S1. TEM images of (a) CeO_2:Nd precursor, (b) CeO_2:Nd@SiO_2, (c)DC/UCNPs, (d) DC/UCNPs@SiO_2-RB/MB, (e) DC/UCNPs@SiO_2-RB/MB/CD36, (f) HRTEM images of DC/UCNPs.

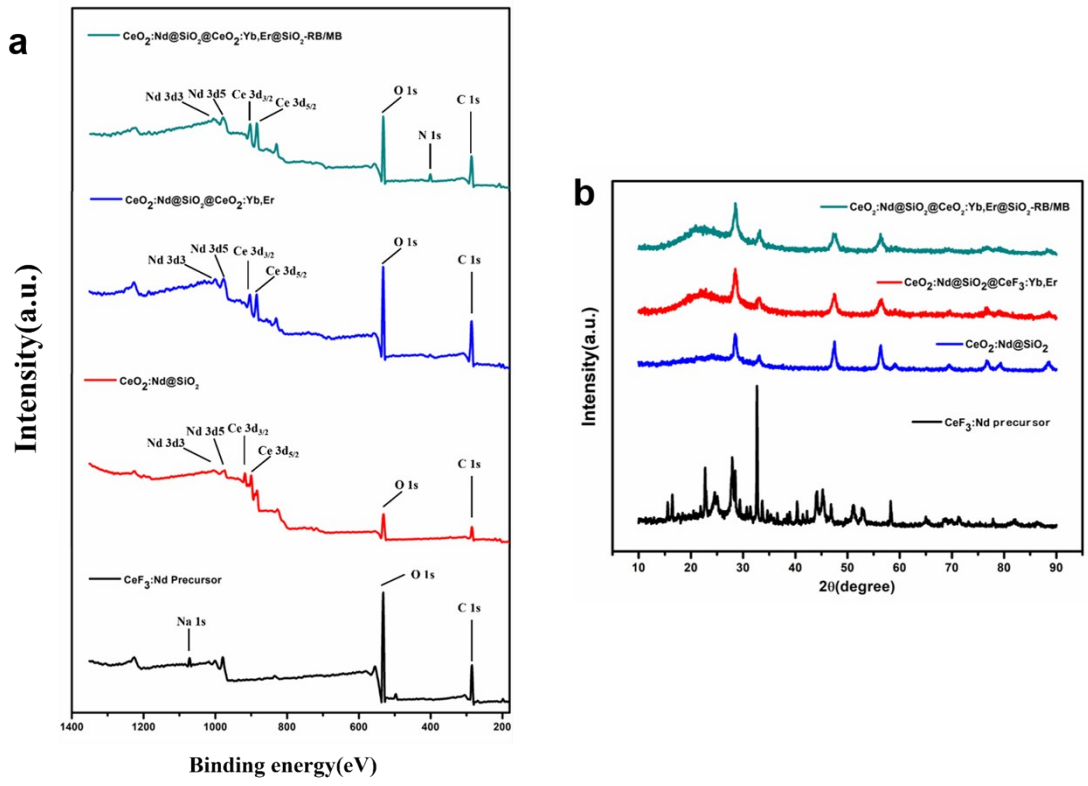

Figure S2. (a) XPS and (b) XRD patterns of as-prepared nanoparticles.

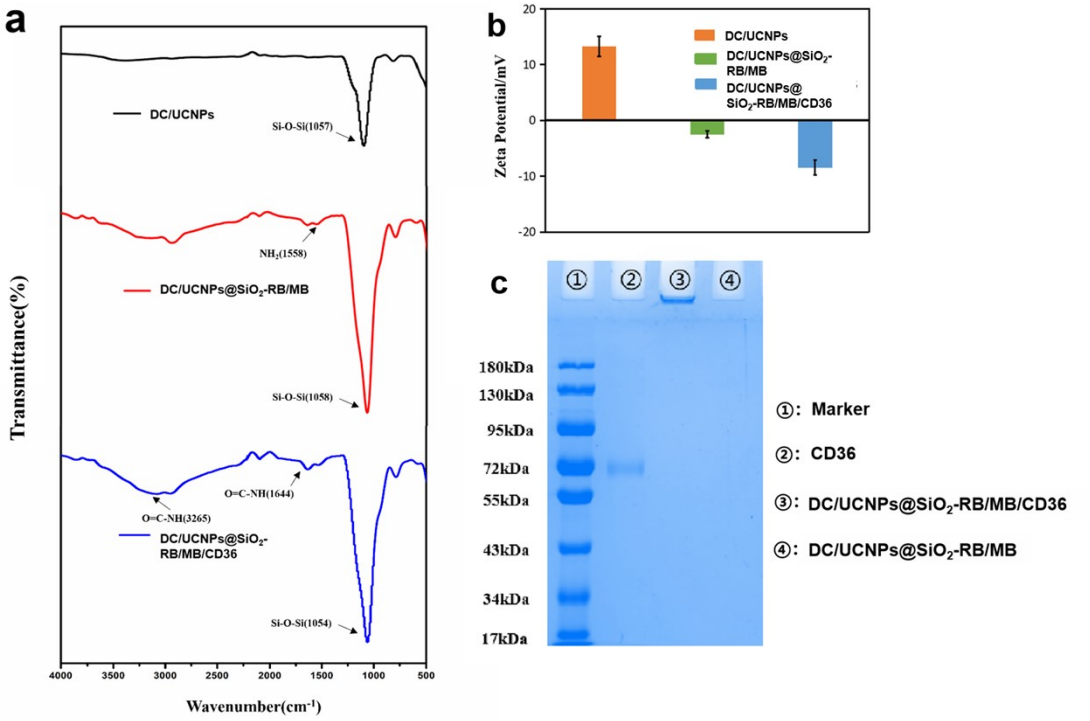

Figure S3. (a) FT-IR spectra and (b) Zeta Potential of as-prepared nanoparticles, (c) SDS-PAGE protein analysis of marker (1), CD36 antibody (2), DC/UCNPs@SiO_2-RB/MB/CD36 (3), and DC/UCNPs@SiO_2-RB/MB (4). Samples were stained with Coomassie Brilliant Blue.

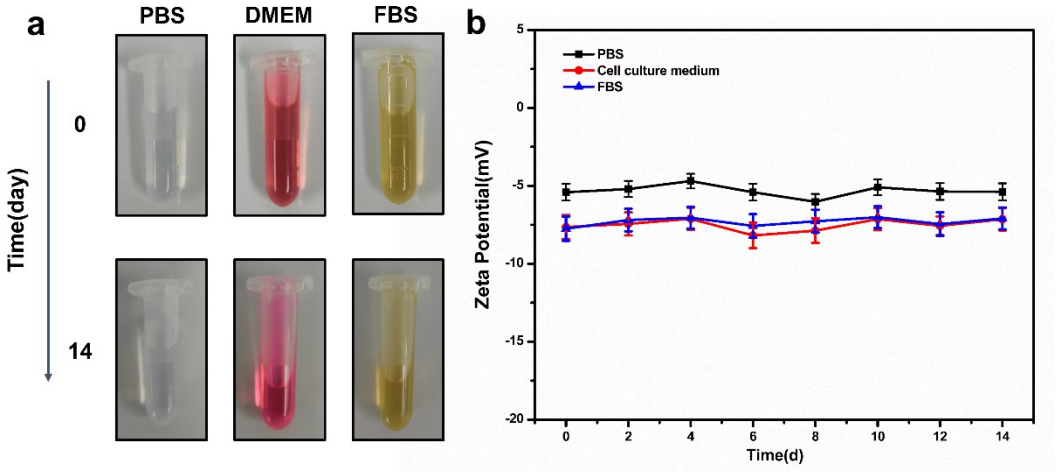

Figure S4. (a) Photographs and (b) Zeta potential data of nanoparticles dispersed in PBS, FBS and cell culture medium (DMEM supplemented with 10% FBS) for 14 days.

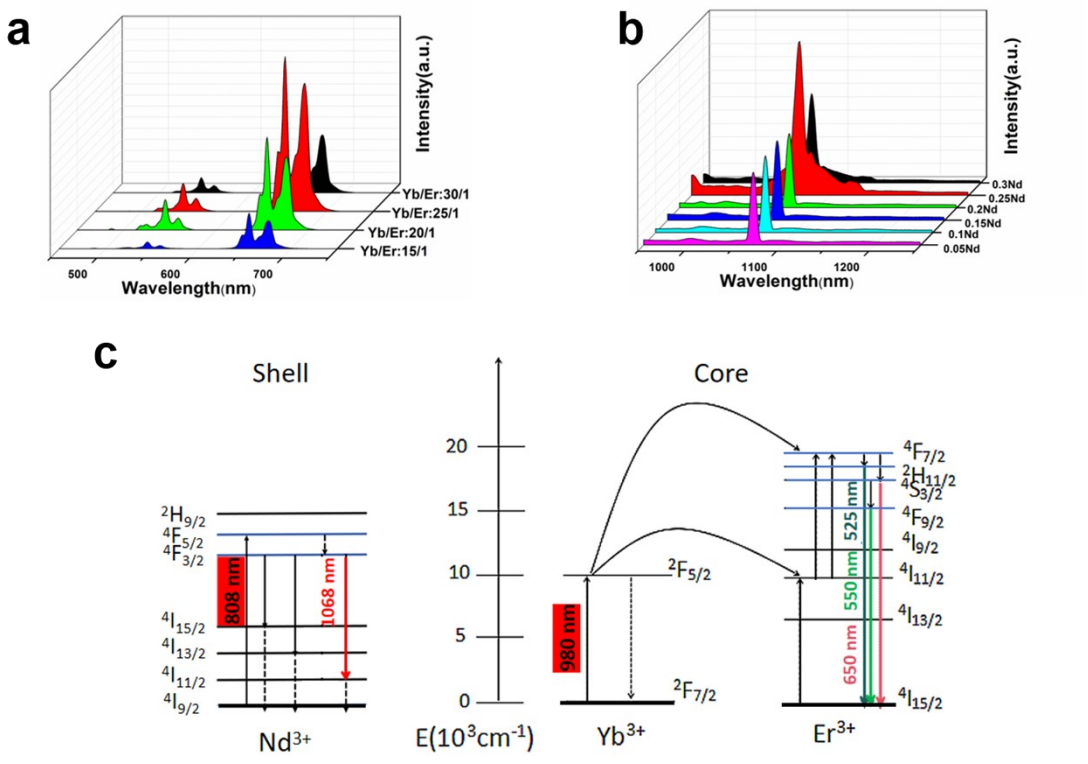

Figure S5. (a) UC and (b) DC emission spectra of DC/UCNPs. (c) Proposed energy transfer mechanisms in DC/UCNPs.

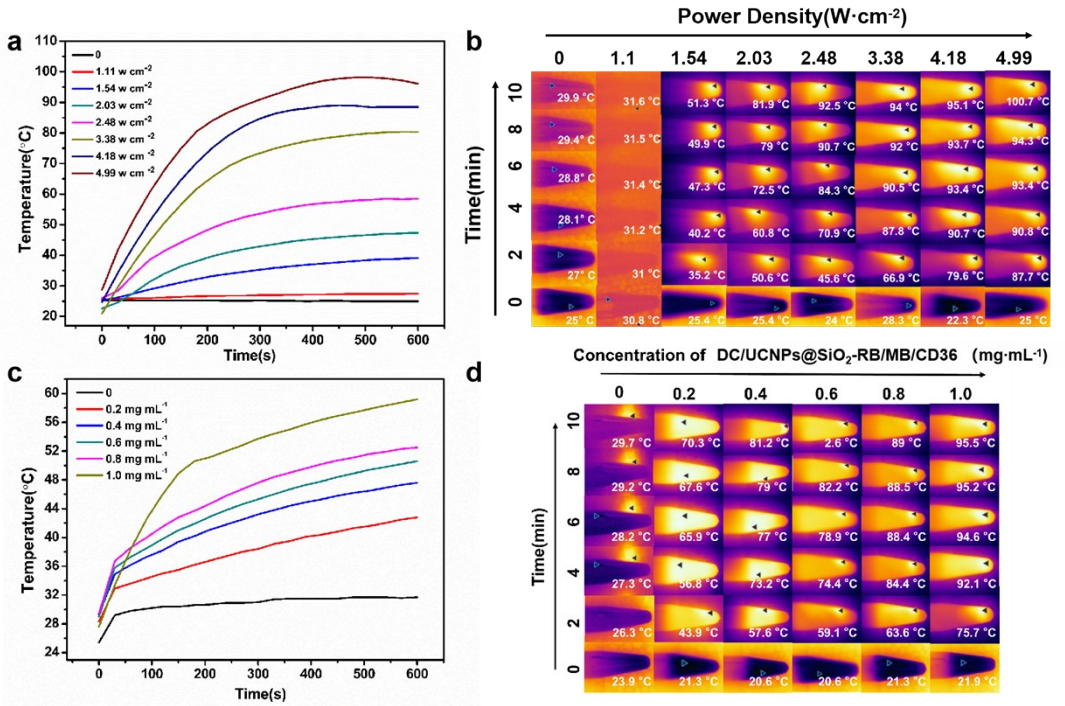

Figure S6. (a) In vitro temperature change curves and (b) Real-time thermal images of

nanoparticles with different laser power density. (c) In vitro temperature change curves and (d) Real-time thermal images of nanoparticles at different concentrations with laser irradiation for 600 s (4.99·W cm^{-2}). For all graphs, data are shown as mean ± S.D. (n ≥ 3).

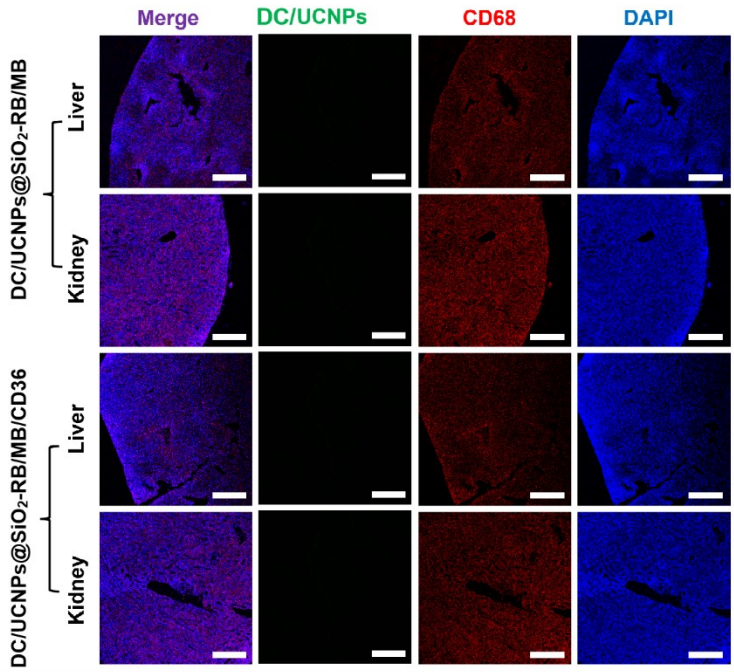

Figure S7. Representative immunofluorescence micrographs of liver and kidney sections of $ApoE^{-/-}$ mice. From the left, DAPI (blue, representing the cell nucleus), CD68 (red, representing macrophages), DC/UCNPs (green, representing DC/UCNPs@SiO_2-RB/MB or DC/UCNPs@SiO_2-RB/MB/CD36) and the merged image. Scale bar: 250 μm.

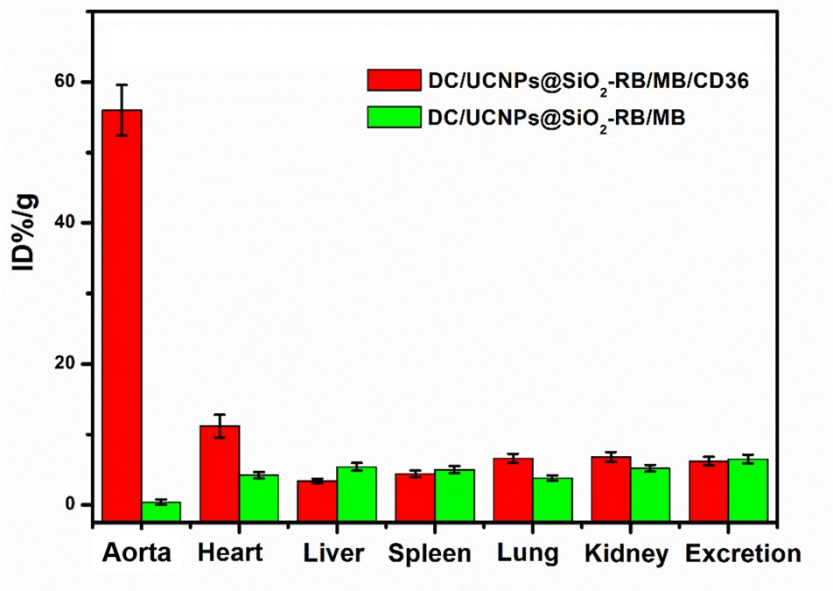

Figure S8. ICP-AES of Ce content in mice after intravenous injection with DC/UCNPs@SiO_2-RB/MB/CD36 (150 μL, 10 mg·kg^{-1}) and DC/UCNPs@SiO_2-RB/MB (150 μL, 10 mg·kg^{-1}).

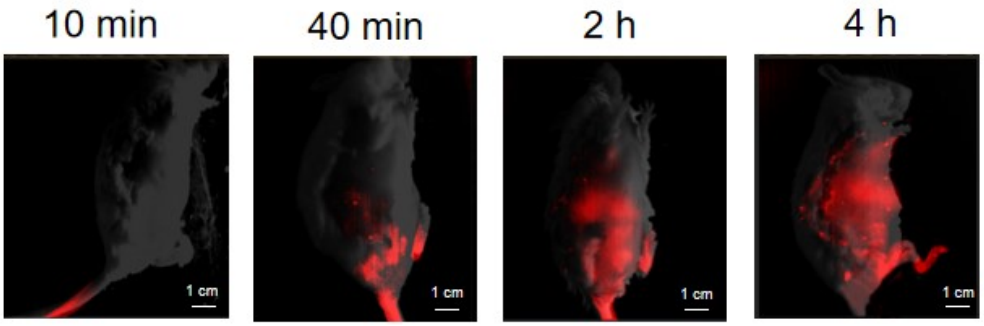

Figure S9. In vivo NIR-II fluorescent imaging of Kunming mice injected intravenously by DC/UCNPs@SiO_2-RB/MB/CD36 solutions (10 mg·kg^{-1}). Scale bar: 1 cm.

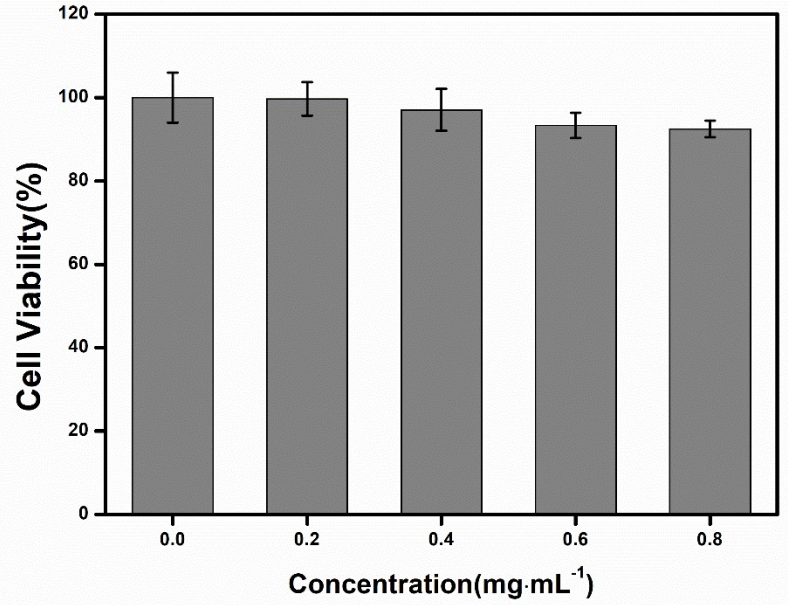

Figure S10. Viability of Normal human hepatocytes after incubation with nanoparticles at different concentrations for 12 h.

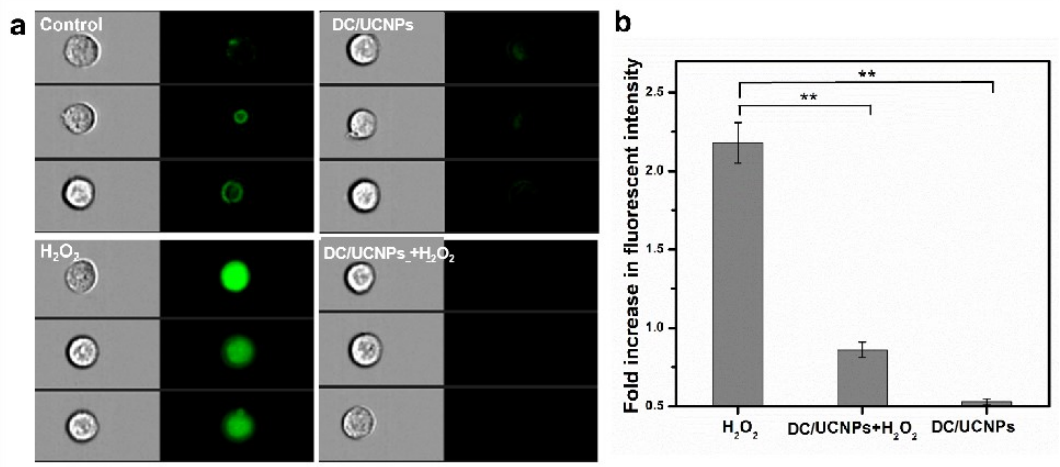

Figure S11. (a) Flow cytometry images of intracellular ROS stained by DCFH-DA with various treatments. (b) Quantification of fluorescence intensity. ***P*<0.01.

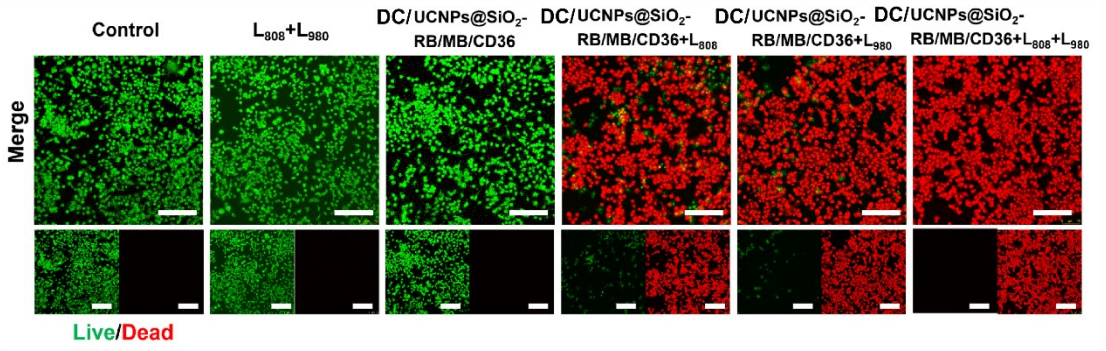

Figure S12. Fluorescence images of live/dead staining of RAW264.7 cells with various treatments. Scale bar: 150 μm.

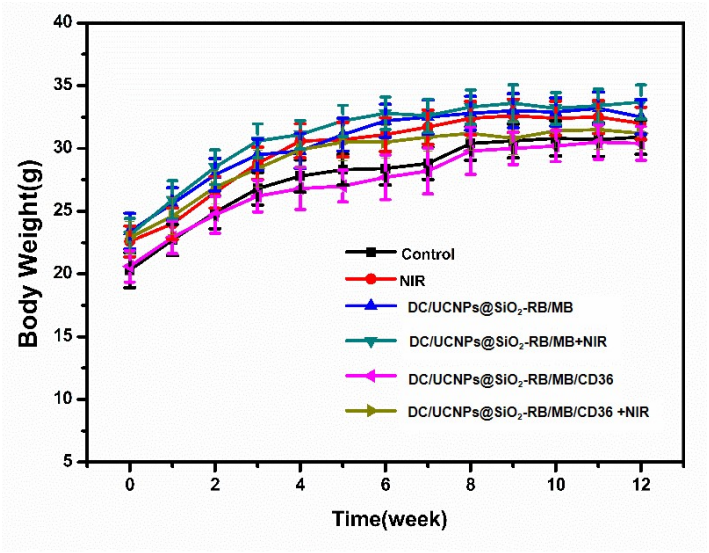

Figure S13. 12-week growth chart of mice from treatment and control (PBS only) groups.

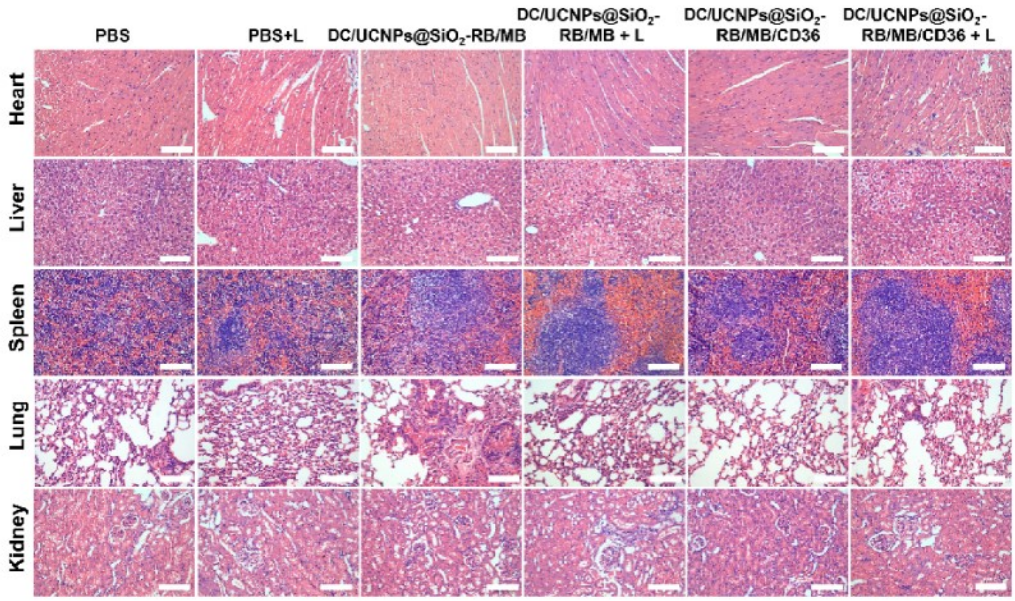

Figure S14. Representative histology (H&E) images of major organs of mice collected from treatment and control groups after 12 weeks. Scale bar: 300 μm.